

A dedicated robust instrument for water vapor generation at low-humidity for use with a laser water isotope analyzer in cold and dry polar regions.

Christophe Leroy-Dos Santos¹, Mathieu Casado^{1,2}, Frédéric Prié¹, Olivier Jossoud¹, Erik Kerstel³, [Morgane Farradèche¹](#), Samir Kassi³, Elise Fourré¹, Amaëlle Landais^{1,*}

¹ Laboratoire des Sciences du Climat et de l'Environnement, CEA-CNRS-UVSQ-Paris Saclay-IPSL, Gif-sur-Yvette, France

² Alfred Wegener Institut, Helmholtz Center for Polar and Marine Research, Potsdam, Germany

³ Laboratoire Interdisciplinaire de Physique, CNRS - Université Grenoble Alpes, Grenoble, France

* corresponding author: amaelle.landais@lsce.ipsl.fr

Abstract

Obtaining precise continuous measurements of water vapor isotopic composition in dry places (polar or high-altitude regions) is an important challenge. The current limitation is the strong influence of humidity on the measured water isotopic composition by laser spectroscopy instruments for low-humidity levels (below ~~3,000~~ 3000 ppmv). This problem is addressed by determining the relationships between humidity and measured $\delta^{18}\text{O}$ and δD of known water standards. We present here the development of a robust field instrument able to generate water vapor, down to 70 ppmv, at very stable humidity levels (average 1σ lower than 10 ppmv). This instrument, operated by a Raspberry interface, can be coupled to a commercial laser spectroscopy instrument. ~~It proved: it turned~~ to be ~~highly~~very stable ~~during in an~~ autonomous ~~operation over mode during~~ more than one year at the East Antarctic Concordia ~~and Dumont d'Urville stations~~station.

1. Introduction

The recent development of laser spectroscopy instruments now enables the continuous measurement of the isotopic composition of water vapor at many observation stations all around the world (Bailey et al., 2015; Bastrikov et al., 2014; Schmidt et al., 2010; Sodemann et al., 2017; Tremoy et al., 2011). In particular, the isotopic composition of the water vapor has proven to be a very useful tool to document moist synoptic events in many locations (Bonne et al., 2014; Guilpart et al., 2017). In polar regions, the water vapor isotopic signal is not only useful to detect the origin of moist air (Bréant et al., 2019; Kopec et al., 2014) but also to improve the interpretation of the isotopic composition of water in surface snow and ice core archives (Steen-Larsen et al., 2014). Indeed, exchanges are occurring after deposition between the surface

snow and the water vapor leading to modifications of the isotopic composition of the former and hence of the archived ice (Casado et al., 2016, 2018; Ritter et al., 2016).

Obtaining continuous measurements of the water vapor isotopic composition at Concordia station in central Antarctica is a key scientific challenge since the deep ice core drilled there, EPICA Dome C, provides the oldest continuous water isotopic record to date (Jouzel et al., 2007). It is thus a key reference for the study of past climate, and a correct interpretation of the isotopic record relies on the quantification of the transfer function between climate parameters and water isotopic composition in ice, itself influenced by exchanges with water vapor in the upper layers of the firn (Casado et al., 2018). Such knowledge is also of uttermost importance for the interpretation of water isotope records from the starting deep drilling project “Beyond EPICA-Oldest Ice” (<https://www.beyondepica.eu>), whose aim is to drill a 1.5-million-year old ice core ~~at~~^{on} the Little Dome C site located 40 km away from Concordia station, hence with similar low temperature and humidity conditions.

One of the main limitations of the current commercial instruments when deployed in polar regions is their relatively poor performance at low water vapor concentration. Generally, the precision of the measured isotopic ratios $\delta^{18}\text{O}$ and δD rapidly worsens when the water mixing ratio decreases to humidity levels below 3,000-5,000 ppmv (part-per-million per volume) (Bonne et al., 2014; Weng et al., 2020). However, in remote continental areas in Greenland and Antarctica, temperatures in winter can drop to very low values, leading to humidity levels down to 10 ppmv (Genthon et al., 2017). Arguably one of the most extreme experiments for continuous measurement of the water vapor isotopic composition was ~~probably~~ the deployment of a commercial Picarro L2130-i instrument at the East Antarctic French-Italian station of Concordia where the mean annual temperature is around -54°C and the humidity barely exceeds ~~1,000-1000~~ ppmv during the warmest summer days (Casado et al., 2016). For such applications, there are two major impacts of low ~~—~~humidity on the raw isotopic signal: first, we generally observe an apparent increase in the $\delta^{18}\text{O}$ and δD with decreasing humidity level and second, the standard deviation associated with the continuous measurements of $\delta^{18}\text{O}$ and δD of the water vapor increases. ~~This~~^{It} can ~~thus~~ lead to overall uncertainties of several ‰ for $\delta^{18}\text{O}$ and tens of ‰ for δD . It is thus of uttermost importance to have a correct determination of the humidity dependency of the water vapor isotopic ratios.

Commercial instruments from Picarro Inc. are usually associated with a Picarro Standard Delivery Module (SDM) ~~designed~~^{dedicated} to generate humidity at stable levels between 5,000 and 30,000 ppmv. Using such a set-up for humidity levels below 5,000 ppmv leads to large uncertainties in the determination of the humidity influence on the water vapor isotopic composition (e.g. Guilpart et al., 2017). These uncertainties are due both to the instability of the water vapor generation using the SDM (in terms of water concentration ~~—~~humidity ~~—~~ and/or isotopic composition) and ~~due~~ to the analytical noise in the spectroscopy measurements when the absorption signals are weak. An alternative commercial device is the LGR (Los Gatos Research) calibration system ([Water Vapor Isotope Standard Source](#)~~water vapor~~

70 ~~isotope standard source~~, WVISS), which uses a nebulizer to instantaneously evaporate micro-droplets of
71 liquid ~~-~~water from a ~~standardstandards~~ reservoir into a large (1 L) vaporizing chamber (Dong and Baer,
72 2010).~~;~~ This system is very stable and well adapted for ~~a~~ humidity range between 2,500 and 25,000 ppmv
73 (Aemisegger et al., 2012).

74 Several home-made water vapor injection systems have been developed with the specific aim to achieve
75 a better stability of the generated humidity at low~~-~~humidity levels. A first approach is to use a dew point
76 generator injecting small amounts of water into dry air (Lee et al., 2005; Wang et al., 2009). This approach
77 is time consuming ~~as it takes long~~ to reach equilibrium and relies on a very precise knowledge of the
78 temperature to ~~quantifycalculate~~ the isotopic fractionation. A method using a piezoelectric microdroplet
79 generator into a dry air stream could generate water mixing ratios ~~at humidity levels~~ between 12 and 3,500
80 ppmv (Iannone et al., 2009; Sturm and Knohl, 2009; ~~Sayres et al., 2009~~). However, adjustment of humidity
81 level and long-term stability were difficult to obtain with such devices. Systems relying on the use of
82 syringe pumps were also built by Gkinis et al. (2010) and Tremoy et al. (2011): a small fraction of the input
83 stream of liquid water is introduced into a hot oven where water is vaporized in the presence of a dry air
84 flow. These systems cover humidity range between 2,000 and 30,000 ppmv. Finally, bubbler systems, in
85 which dry air flows through a large volume of water to create saturated vapor, are very robust but can
86 only produce water vapor at high~~-~~humidity ~~levelslevel~~ (Ellehoj et al., 2013). The aforementioned devices
87 are unfortunately not well suited for automatic long-term operation at low~~-~~humidity levels. During the
88 2014-2015 summer field season at Concordia station in Antarctica, a home-made humidity generator
89 specifically designed for low~~-~~humidity levels (Landsberg, 2014) has been deployed (Casado et al., 2016).
90 The device used dual high-precision, low-volume, syringe pumps to generate stable humidity levels at two
91 different isotopic compositions over the range from 100 to 800 ppmv (Casado et al., 2016). Unfortunately,
92 we observed quite a large scattering among the isotopic values measured at similar humidity levels, as
93 well as a large discrepancy between the humidity dependency of the water isotopic ratios measured in the
94 field and ~~the one that~~ measured in the laboratory. Upon return to the laboratory, these defaults were
95 traced primarily to tiny leaks in the water supply lines to the syringes.

96 -Therefore, we re-engineered the prototype by Landsberg (2014) in order to develop a robust and
97 autonomous device for stable low~~-~~level humidity generation for the purpose of precise humidity
98 calibration of spectroscopic instruments. ~~Such devices have~~~~This device has~~ now been operating with
99 minimum manual intervention for more than one year at two polar stations in Antarctica, Dumont d'Urville
100 and Concordia, coupled to Picarro laser spectroscopy instruments. We detail here the technical description
101 of the instrument and show key performance characteristics, enabling, for instance, a discussion of small
102 amplitude signals such as the diurnal variability of the water vapor isotopic composition in remote dry
103 sites in East Antarctica.

2. New vapor generator for low-humidity levels

The low-humidity level generator (LHLG) developed here relies on the same principle as the one developed by Landsberg (2014), i.e., a steady, undersaturated evaporation of a liquid water droplet at the tip of a needle into a dry air stream inside a small evaporation chamber. Based on this first prototype, the instrument has been remodeled including a specific hardware and software design.

2-1-Physical principle

The LHLG is based on undersaturated evaporation of a small droplet at the tip of a needle (Figure 1). Liquid water is pushed through a needle around which dry air is flowing. Dry air is obtained from a bottle of high purity synthetic air with pressure regulation through two manometers connected in series. The mass flux of water f_L is kept low compared to the air mass flow f_A so that the relative humidity RH of the downstream moist air flow remains low ($RH < 0.1$). Therefore, the air stays largely undersaturated and its humidity is controlled only by the flow of liquid water in the needle and that of the dry air upstream of it. The mixing ratio (or humidity) of the air as classically provided by a Picarro instrument is given by:

$$MR = \frac{d_{H_2O} \times f_L \times R \times T_{st}}{f_A \times P_{st} \times M_{H_2O}} \quad (\text{eq. 1})$$

where $d_{H_2O} = 1000 \text{ kg} \cdot \text{m}^{-3}$ is the density of water, $R = 8.314 \text{ J mol}^{-1} \text{ K}^{-1}$ is the universal gas constant, $T_{st} = 293.15 \text{ K}$ and $P_{st} = 1013.25 \text{ hPa}$ are standard conditions of temperature and pressure and $M_{H_2O} = 18.10^{-3} \text{ kg} \cdot \text{mol}^{-1}$. Note that the flow of water f_L needs to be expressed in $\text{m}^3 \cdot \text{min}^{-1}$ and the air flow f_A is expressed in $\text{m}^3 \cdot \text{min}^{-1}$ at 20°C and 1 atm (standard cubic meter per minute).

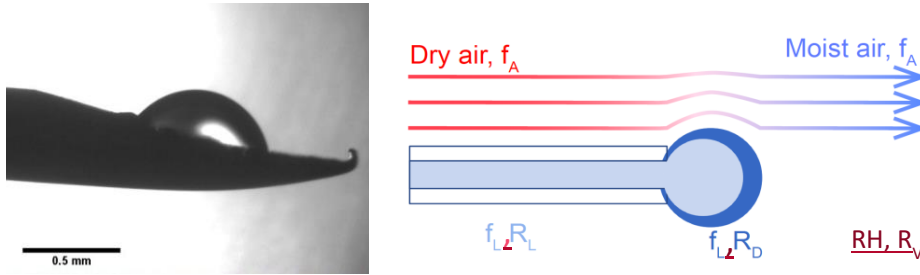


Figure 1: Evaporation of a droplet in the humidity generator chamber: left, picture from the prototype from Landsberg (2014); right, schematics of the water molecules being transferred to the air flow (Casado, 2016).

Physically, when the flux of water or air is changed, there is first a transient regime during which the radius of the droplet changes, modifying the evaporative surface and therefore the humidity of the outgoing air. Once a stationary regime is reached, the radius of the droplet is stabilized and the humidity is given by equation 1. In this regime, there is no accumulation of water molecules in the system and therefore the isotopic composition of the vapor produced is equal to the isotopic composition of the liquid water injected in the needle: $R_V = R_L$ (note that because of the fractionation during the transition phase, the isotopic composition of the droplet R_D is ~~necessarily~~ different from R_L and R_V , [see Kerstel, 2020](#)). When changing the flux of evaporating water, we modify the size of the evaporating surface and therefore the radius of the drop. The evolution of the radius of the drop can be obtained from the resolution of a non-linear differential equation of the volume V of the drop:

$$dV/dt = f_L - f_{evap} \quad (\text{eq. 2})$$

where $f_{evap} = k_e \times S$ is the evaporation flux depending of k_e , the evaporation rate, and S , the surface area of the drop exposed to the dry air. A good approximation is to consider the shape of the drop as a fraction of a sphere of variable radius intercepted by the surface of a disk of constant radius (the syringe tip). By solving numerically the differential equation (2), it is possible to faithfully simulate the behavior of the device under changing conditions [\(Kerstel, 2020\)](#). ~~The isotopic composition is computed by the introduction of an evaporation fractionation factor following Cappa et al. (2003).~~ This numerical approach validates the theoretical explanation of the undersaturated evaporation of the droplet. ~~Importantly, it#~~ is noted that in steady-state [as is the case for our application](#), the isotopic composition of the generated [humid air is identical to that of the injected water stream, and therefore](#) ~~vapor~~ does not depend on the ~~infusion rate injected flux of water~~, nor on the specific humidity.

2-2- Instrument conception

- Technical realization

As the LHLG relies on operating in a stationary regime, it is important that the dry air input and the water input are steady. Thus, the air and water fluxes, as well as the air pressure in the evaporation chamber are controlled by electronic PID regulators. [Temperature intervenes through its effect on fractionation and the evaporation rate \(apart from a negligible effect on the flow controller stability\), which could lead to a departure from steady-state operation. For these reasons, the temperature of the evaporation chambers was maintained at 20°C \(within 1°C over 24 hours\).](#)

The dry air flux is regulated by a high-precision mass flow controller (Vögtlin GSC-A9TS-DD22), [that has an](#) operating ~~at a~~ range from 6 to 600 sccm (std cm³ min⁻¹) and an accuracy of 3.3 sccm. The water flux is

regulated by a high-precision syringe pump (Harvard Apparatus Pump 11 Pico Plus Elite Dual), which can produce a water flow down to 10.8 pL min^{-1} with an accuracy of 0.35 % using syringes with a volume ranging from 10 μL to 250 μL . We operate in the routine mode with a dry air flow of 300 sccm and a water flow between 0.02 to 0.5 $\mu\text{L min}^{-1}$ using mainly 50 or 100 μL syringes. A ~~syringesingle~~ pump is equipped with two syringes that provide two water flows into two evaporation chambers in parallel (~~Figure~~~~Figures~~ 2~~and 3~~). Each syringe is connected to a water reservoir and to an evaporation chamber by a double 3-way liquid valve (Rheodyne MXX777603) switching from an “infuse” mode to a “~~withdraw~~” ~~mode to refill the syringes. The water in the water reservoirs is sampled every month to check its isotopic composition and renewed when the level of water is below half the maximum level. A maximum evolution of the isotopic composition of the lab-standard filling the water reservoirs has been observed as 0.05‰ and 0.5‰ respectively for $\delta^{18}\text{O}$ and δD over a 2-month period. refill~~” mode.

A major change to the instrument designed by Landsberg (2014) is the introduction of ~~the~~~~this~~ double 3-way valve with leak~~-~~tight connections and an internal volume of 1.9 μL . This modification is an important improvement as it enables automatic handling of the ~~lab~~-standards from a reservoir to the evaporation chamber with a robust connection, avoiding in particular potential air bubbles in the water flow. Indeed, the compressibility of air bubbles trapped in the water flow can lead to flow irregularities by amplification of small non-linearities in the progression of the syringe plunger. This ~~would~~~~will~~ lead to non-steady state operation, which in turn ~~would create~~~~creates~~ artefacts in the humidity and isotopic composition, reducing the performance of the calibration device (~~see Kerstel 2020~~). In addition, the 3-way valve provides the opportunity of a “~~withdrawn~~~~refill~~” mode in which the syringes draw ~~lab~~-standard water from a reservoir. When equipped with 100- μL syringes, the instrument can operate for several hours up to one day between refills. With the addition of the auto-refill option and the effective suppression of bubbles, the instrument can be used unattended for many months, as required for an Antarctic winter field campaign.

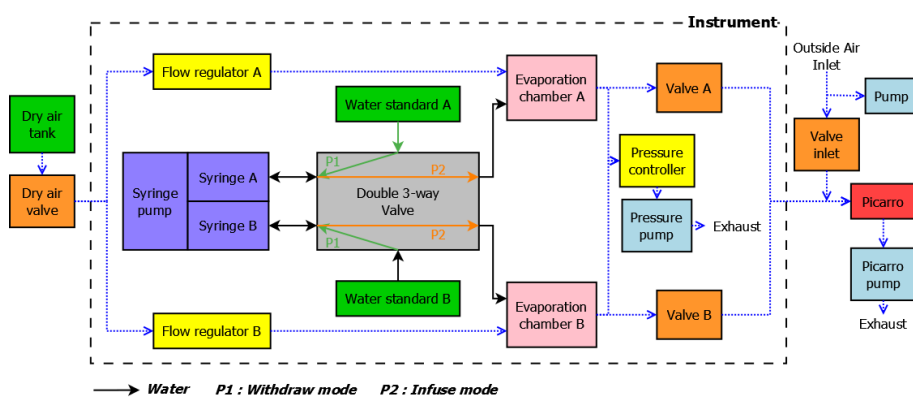
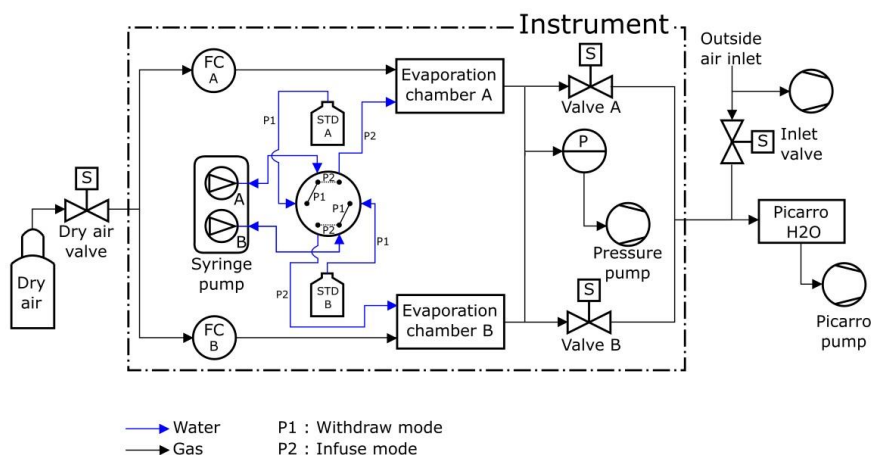


Figure 2: Humidity generator schematic diagram [\(see supplementary Table S1 for details on the different elements\)](#)

The evaporation chambers are stainless steel cylinders equipped with specific connectors (Swagelok Ultra-Torr SS-4CD-TW-25) holding silicon rubber septa through which needles are inserted toward the middle of the chamber. The pressure in both chambers is regulated by a pressure controller (Bronkhorst P-702CV-1K1A-AAD-22-V) with a precision of 3 mbar in a range from 0 to 1,000 mbar. This pressurization of the two chambers combined with the relatively high flow (higher than required by the infrared spectrometers) enables maintaining a steady state whether or not the infrared spectrometer is connected, and increases the time efficiency of calibration procedures. The spectrometer is not sensitive to the inlet pressure, the precision of the pressure controller is not an essential aspect. On the contrary, the precision of the flow controller is key for the precision of the humidity level produced by the instrument: it is of 1% for the air

flow which is comparable to the precision of the measurement of the humidity level with the optical spectrometer. When the instrument is connected to the infrared spectrometer, the excess humid air flow is exhausted to the room through the pressure pump and the spectrometer only pumps what is required (Figure 2). The control of the instrument is ensured by a Raspberry Pi that can be interfaced to the L2130-i in sequencer mode (see below).

The control of the instrument is ensured by a Raspberry Pi that can be interfaced to a Picarro water analyzer (L2130-i in our case) in sequencer mode (see below). The hardware has been designed to meet the specifications dictated by field conditions: 1) All components are fixed in a transportable case (except the dry air bottle), isolated from vibration by an anti-vibration foam. 2) A panel of connectors (HDMI, USB, Ethernet, etc.) ensures the accessibility to the instrument when it is closed. 3) The electrical and electronic parts (e.g. power supply, Raspberry Pi) are separated from the rest of the instrument (e.g. sensors, gauges). Both the electrical and electronic parts are fully and easily accessible in case of failure.

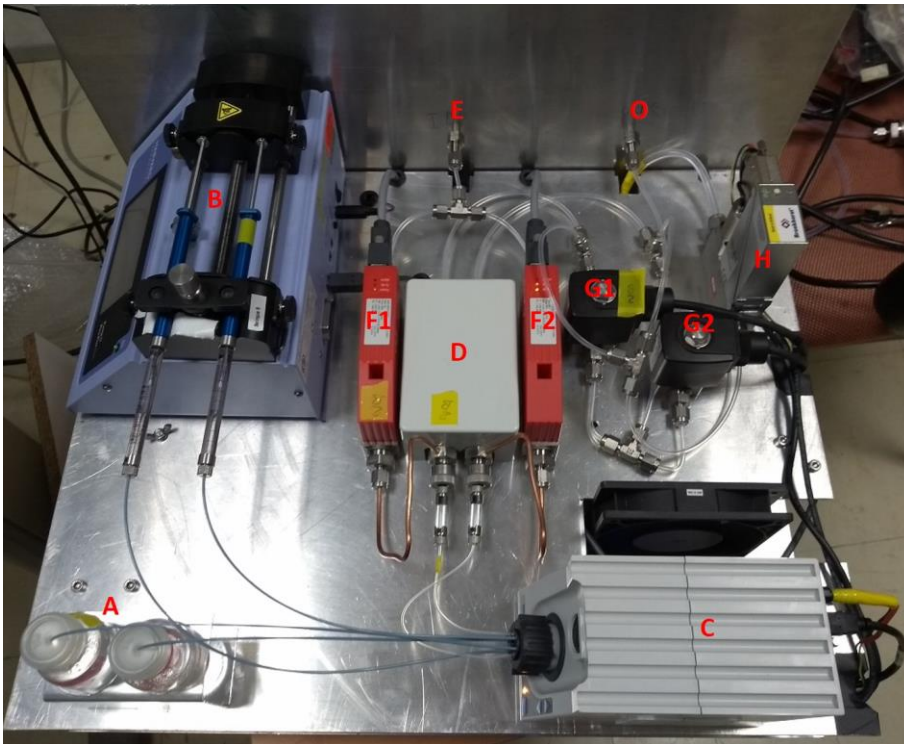


Figure 2: Picture of the upper stage of the instrument with the main fluidic parts. Two water standards (A); a dual syringe pump (B); a double three-way valve (C); two evaporation chambers (D); an input of dry air (E); two high-precision mass flow controllers (F1 & F2); two electrovalves (G1 & G2); a pressure controller (H); an outlet (O).

- Software details

The control software has been developed using open source Python libraries and homemade drivers, including a user interface displaying the state of relevant components and the value of the different sensors. The software (HumGen) can be downloaded on line (<https://github.com/ojsd/humgen>; <https://doi.org/10.5281/zenodo.4003465>).

The LHLG can operate in eight different states, each state representing a specific setup for each element (valves position, syringe pump infusion rate, dry air flow rate, pressure). Those eight states can be divided into three categories: a routine~~simple~~ mode, an expert mode and a humidity dependence calibration mode. The simple mode is composed of six predefined states referring to the classic~~classical~~ isotopic calibration in everyday routine operation (Table 1): 1) measurement of the outside air water vapor isotopic composition; 2) drying of the cavities; 3) “humidity boost”, in order to reach faster the desired humidity level in the cavities; 4) injection of the standard A in the corresponding evaporation chamber at a set humidity level; 5) injection of the standard B in the corresponding evaporation chamber; 6) refill of the syringes. The expert mode is useful to adjust each parameter manually: flow rates on the controllers FCA~~F1~~ and FCB~~F2~~, opening of the electrovalves AG~~1~~ and BG~~2~~, mode (infuse~~injection~~ or withdraw~~refill~~) and infused rate for the syringe pump, pressure regulation, state of the double three-way valve, activation of the pressure~~vacuum~~ pump at the exhaust, opening of external electrovalves from the dry air tank and to the inlet (Figure~~Figures~~ 2 and 3). The humidity dependence calibration mode produces a scale of increasing humidity steps in the evaporation chambers (e.g. from 100 ppmv to 1000 ppmv, through steps of 100 ppmv for 50 minutes for each standard). The details of the sequence (standard type, humidity level and duration of each step) is defined in a text file by the operator from the Raspberry interface, the Raspberry being itself connected to Ethernet for remote access.

The Picarro L2130-i analyser has an External Valve Sequencer, which is able to turn on/off up to six electrovalves and create loop sequences with defined durations for each step of the sequence. This tool can be diverted from its original purpose by using it as a 6-digit code: each of the humidity generator~~generator's~~ state is associated with a code. When the Picarro~~Picarro's~~ Valve Sequencer matches one of the state~~state's~~ code, this state is triggered on the humidity generator. This eases both the operator's activities and the data post-treatment, because the current valve status - thus the calibration instrument state - is saved in the analyzer output data file, in the "ValveMask" column. The Raspberry inside the LHLG reads the Valve Sequencer state code using the Picarro's Remote Control Interface (a RS232 serial connection through one of the rear-face DB9 connector).

States (min)	Flow <u>FCA</u> (sccm)	Flow <u>FCB</u> (sccm)	Valve <u>AG1</u>	Valve <u>BG2</u>	Syringe Pump (μL/min)	Inlet Valve *	Dry air <u>Valveval</u>	Pressure controller (mbar)	Pressure Pump for exhaust	Double 3-way valve
Outside air (1100)	0	0	Closed	Closed	0	Open	Closed	Off	Off	To chamber
Drying (20)	400	400	Open	Open	0	Closed	Open	Off	Off	To chamber
Boost (0.7)	300	300	Open	Open	Infuse at 2.5	Closed	Open	905	On	To chamber
Standard A (50)	300	150	Open	Closed	Infuse at 0.25	Closed	Open	905	On	To chamber
Standard B (50)	150	300	Closed	Open	Infuse at 0.25	Closed	Open	905	On	To chamber
Reset (1)	Closed	Closed	Closed	Closed	Withdraw max speed	Open	Closed	Off	Off	From standard

Table 1: Typical routine sequence of measurements + calibration for two standards A and B at 1000 ppmv for a measurement site located at sea level. No mixing occurs between standards A and B during steps "Standard A" and "Standard B" (see supplementary text S1).

Note that the humidity dependence mode and the expert mode can also be included in the valve sequencer but are not used in a daily calibration routine. ~~*) The Inlet Valve is placed outside the vapor generator instrument; when open it enables the measurement of outside air.~~

A set of tools has been developed to quickly check daily calibration. In the field, analyzer and LHLG data are archived daily and sent to the laboratory, i.e. at LSCE, Gif sur Yvette. They are checked semi-automatically once a week to warn maintenance personnel in the event of a malfunction.

3- Performance of the instrument

While the stability of the instrument has been tested over a large range of parameters (supplementary Table S2), air flow and infusion rate have been adjusted to optimize the stability of the generated vapor while minimizing the dry air consumption. The LHLG is able to generate stable levels of humidity (drift lower than 20 ppmv over one hour and 1σ below 10 ppmv over 10 minutes), ranging from 70 ppmv to 2,400 ppmv following the optimal set-points shown in Table 2. ~~2300 ppmv.~~

Humidity (ppmv)	Infusion rate ($\mu\text{L}/\text{min}$)	Dry Air flow (sccm)
80	0.01	300
160	0.02	300
320	0.04	300
800	0.1	300
1200	0.15	300
1600	0.2	300
2400	0.3	300

Table 2: Set-points for water infusion rate and dry air flow at a temperature of 20°C.

3-1- No fractionation during water vaporization in the cavity

We have checked that there was no fractionation of the water during its transfer from the bottles to the syringe pump, then from the syringe to the moist air generated in the vaporization chamber through the following tests. ~~The isotopic composition of three different standards have been compared, generated by the present LHLG as well as the commercial SDM, both at a humidity of 2,000 ppmv over 40-min time spans. The measured $\delta^{18}\text{O}$ and δD excess values agreed to within 0.2‰ and 1‰, respectively, for the 3 standard waters. Note that 2,000 ppmv is close to the upper value of the present LHLG (2,300 ppmv) while it is the very low one of the SDM (see Fig. 6 of section 3-2).~~

First, the isotopic composition of three different lab-standards calibrated against VSMOW at LSCE (H_2O - CO_2 equilibration followed by IRMS for $\delta^{18}\text{O}$; Cavity RingDown Spectroscopy for δD ; calibrated every 3 years using VSMOW and VSLAP provided by IAEA) have been compared, after their generation by the present LHLG and by the commercial SDM, both at a humidity of 2,000 ppmv over 50-min time spans. The measured $\delta^{18}\text{O}$ and δD values agreed to within 0.5‰ and 2‰, respectively, for the 3 lab-standard waters calibrated against VSMOW: EPB ($\delta^{18}\text{O} = -6.24$ ‰; $\delta\text{D} = -43.6$ ‰), NEEM ($\delta^{18}\text{O} = -33.50$ ‰; $\delta\text{D} = -257.2$ ‰), FP5 ($\delta^{18}\text{O} = -48.33$ ‰; $\delta\text{D} = -383.5$ ‰). Second, the measured isotopic composition of the same standard (FP5) generated at different humidity levels between 1,000 and 2,400 ppmv by the SDM and the LHLG show the same $\delta^{18}\text{O}$ (δD) evolution with humidity within respective uncertainties (Supplementary Figure S1).

3-2- Stability of the water vapor delivery

Mis en forme : Police :Gras, Soulignement

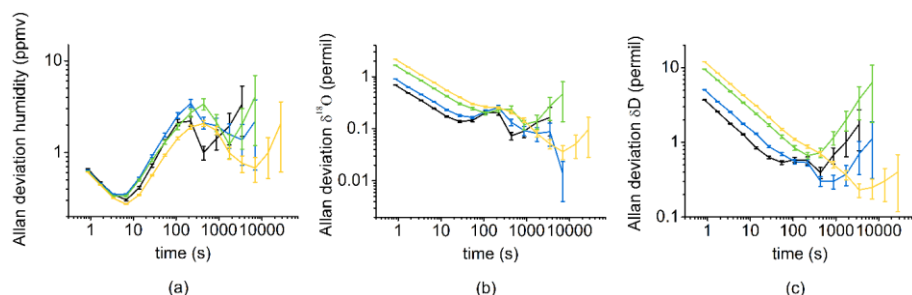


Figure 3: Allan variance over 4 hours for different humidity levels (black 1,080 ppmv; blue 770 ppmv; green 400 ppmv; yellow 320 ppmv) for humidity (a), $\delta^{18}\text{O}$ (b) and δD (c).

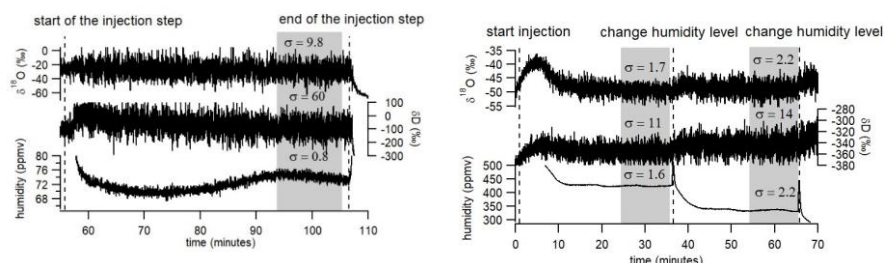


Figure 4: Records of $\delta^{18}\text{O}$, δD and humidity over 3 humidity plateaus (72 ppmv on the left, 425 and 335 ppmv on the right) obtained with the LHLG- (December 2018 at Concordia). The grey rectangles indicate the period (10 min) over which the average values are kept for calibrating the data generated by the L2130-i analyzer.

Figure 3 displays the Allan variance in $\delta^{18}\text{O}$, δD and humidity over 4 hours for different humidity levels. The humidity variance always stays below 10 ppmv over the 4 hours test and the $\delta^{18}\text{O}$ / δD Allan variances display minimum values below 0.1 ‰ and 0.8 ‰ respectively (the Allan variance of $\delta^{18}\text{O}$ and δD are however strongly dependent on the analyzer and on the humidity level). In the routine mode (Figure 4), we perform plateaus of 30 to 50 minutes (50 minutes when the instrument is unattended since the time to reach the plateau varies between a few minutes to 30 minutes). We thenFigure 4 displays the performance of the instrument at different low humidity levels (72, 425, and 335 ppmv). In the routine mode, we select the last 10 minutes before the following switch of the instrument to measure the average level of humidity and the isotopic ratios, $\delta^{18}\text{O}$ and δD . We also calculate the associated standard deviations and reject the values if the humidity standard deviation exceeds 30 ppmv over these last 10 minutes. In Figure 4, one observes that the standard deviations for humidities generated in the routine mode are

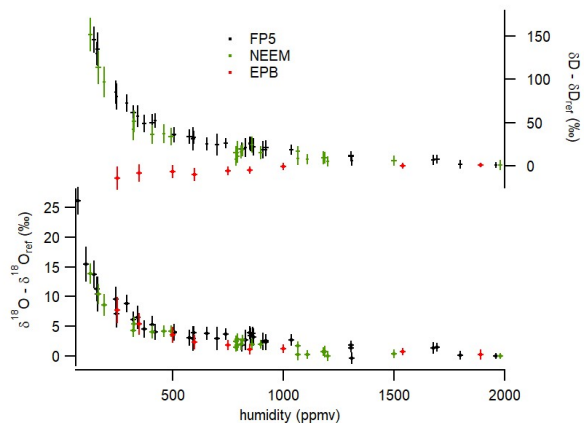
Mis en forme : Police :NimbusSanL-Regu, Couleur de police : Accent 1

Mis en forme : Ne pas ajuster l'espace entre le texte latin et asiatique, Ne pas ajuster l'espace entre le texte et les nombres asiatiques

actually much lower, ~~in the 2 ppm range~~. The corresponding standard deviations for the isotopic ratios ($\delta^{18}\text{O}$ and δD , see values indicated in Figure 4) increase with decreasing humidity, reflecting the decrease of the molecular absorption signal ~~decrease~~ recorded by the ~~L2130-L2130-i~~ laser ~~analyzers~~ analyzer. This has an obvious impact on the determination of the relationship between humidity and water vapor isotopic composition.

The performance of the present LHLG can be compared to the performance of the SDM (see Supplementary Figures S1 and S2). ~~First (Figure S2), a~~ For such comparison has been performed at a humidity level of 800 ppmv, for which, ~~we have numerous~~ used daily calibrations performed with a SDM ~~from, in a routine mode, during~~ a 4.5 years field deployment in Svalbard (Leroy-Dos Santos et al., 2020). ~~Over the full series, we kept only the 10 minute plateaus where standard deviation associated with humidity variations during calibration was below 150 ppmv. The best result at low humidity over the full period was a standard deviation σ of 31 ppmv over 10 minutes at 500 ppmv. Standard deviation largely increases when humidity decreases. This best SDM performance displays significantly below the performance of the LHLG, which is a standard deviation 1σ of 31 ppmv, which is significantly worse than the performance of the LHLG (standard deviation 1σ ~~lower than 10 ppmv~~ on average and ~~down to a~~ ~~1 σ of 2 ppmv~~ for 30% of the generated humidity plateaus). Second (Figure S1), while we measure the same influence of humidity on measured $\delta^{18}\text{O}$ and δD either with the SDM or with the LHLG, the 1σ values on humidity levels are much larger for the SDM than for the LHLG.~~

3-3- Determination of the influence of humidity on water vapor isotopic composition



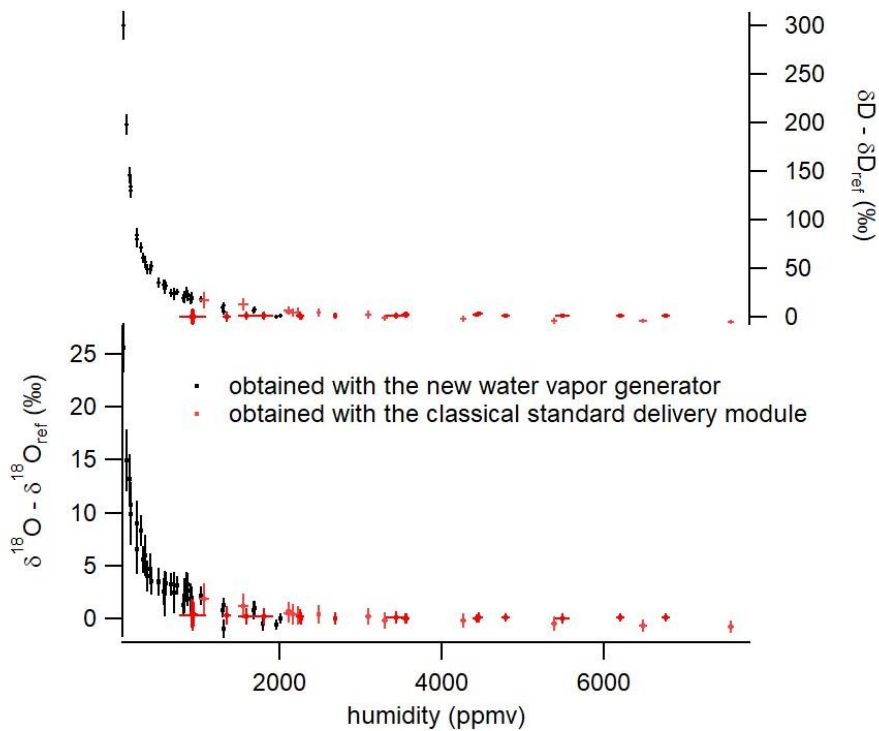


Figure 5: Influence of humidity on the isotopic composition ($\delta^{18}\text{O}$ and δD) of the vapor obtained with ~~the~~ SDM (red) and with our new LHLG with 3 water lab-standards (black). The error bars are calculated as the standard deviation (1σ) over the generated values by the L2130-i instrument during 10 minutes at 1 second resolution (i.e. without any pre-averaging of the raw dataseres). The $\delta^{18}\text{O}_{\text{ref}}$ and $\delta\text{D}_{\text{ref}}$ are the ~~true~~ reference values of the injected water standards at 2,000 ppmv.

Contrary to the commercial SDM, which hardly produces stable and reproducible humidity levels below 500 ppmv, the LHLG was able to daily produce stable 10-minute humidity plateaus over the range from 70 ppmv to 2,400,000 ppmv with an associated standard deviation of the order of lower than 10 ppmv over more than one year at the Concordia ~~and Dumont d'Urville stations~~ (installation in December 2018). The stability of the LHLG allows a robust quantification of the L2130-i analyzer drift thanks to a daily measurement of the same water isotopic standard reference (see Table S3 showing actually no measurable drift over a 3-week period). It also permits the characterization of the measurement non-linearities observed at low-humidity (Figure 5). The more than one-year long Concordia ~~and Dumont d'Urville datasets~~ showed that the humidity dependence of $\delta^{18}\text{O}$ and δD did not vary measurably. The uncertainty of the obtained calibration curve can be attributed entirely to the L2130-i

355 $\delta^{18}\text{O}$ and δD measurements. In other words, the uncertainty bars in the horizontal (x-) axis in Figure for the
 356 black curve in Fig. 5, associated with the LHLG, are negligible.
 357 Our data show a result already observed in Weng et al. (2020): while the dependency of $\delta^{18}\text{O}$ and δD to
 358 humidity is similar for low $\delta^{18}\text{O}$ and δD lab-standards (NEEM and FP5), we observe a different behavior for
 359 the δD vs humidity relationship for the high $\delta^{18}\text{O}$ and δD lab-standard EPB. This result strengthens the
 360 recommendation of Weng et al. (2020) to use two water standards in the range of the measured water
 361 vapor isotopic composition to best calibrate our final data. In our case, our applications were in Antarctica,
 362 so that we used our two lowest lab-standards (NEEM and FP5). For the two standards and for this particular
 363 Picarro L2130-i (results are expected to depend on the instrument), the same dependency of isotopic
 364 composition vs humidity is observed. We express this dependency as the relationship between the
 365 difference in δD or $\delta^{18}\text{O}$ between the measured value at the given humidity and the value of the same
 366 standard measured at a humidity of 2,000 ppmv. The experimental data for NEEM and FP5 from Figure 5
 367 are fitted through polynomial functions with respect to humidity h (in ppmv):

368
$$\delta^{18}\text{O} - \delta^{18}\text{O}_{\text{ref}} = 3.97 \times 10^{-18} \times h^6 - 3.59 \times 10^{-14} \times h^5 + 1.28 \times 10^{-10} \times h^4 - 2.31 \times 10^{-7} \times h^3 + 2.19 \times 10^{-4} \times h^2 - 1.06 \times 10^{-1} \times h + 23.7 \text{ (eq. 3)}$$

370
$$\delta\text{D} - \delta\text{D}_{\text{ref}} = 6.86 \times 10^{-17} \times h^6 - 6.00 \times 10^{-13} \times h^5 + 2.08 \times 10^{-9} \times h^4 - 3.61 \times 10^{-6} \times h^3 + 3.31 \times 10^{-3} \times h^2 - 1.54 \times h + 313 \text{ (eq. 4)}$$

374 After this correction, the measured values corrected from humidity dependence are corrected using the
 375 comparison of the measured values of the 2 standards at 2,000 ppmv to their VSMOW calibrated values
 376 as explained in section 3.5 below.

358 3.5- Accuracy of the system

379 The accuracy of the system has been addressed performing a 2-standard calibration and measuring a third
 380 standard treated as an unknown. We used two lab-standards calibrated vs VSMOW with large $\delta^{18}\text{O}$ and
 381 δD differences (EPB and FP5) and used the lab-standard NEEM, also independently calibrated against
 382 VSMOW. The 3 lab-standards have been vaporized at 800 ppmv and measured by the same L2130-i
 383 analyzer.

Standard Date	VSMOW calibrated value Humidity (ppmv)	Measured value at 800 ppmv $\delta^{18}\text{O}$ (‰)	Measured value corrected from humidity dependence (Equation 1) δD (‰)
16-December-2019	380	-32.0	-207
17-December-2019	369	-31.9	-210

Mis en forme : Police : +Corps (Calibri), 11 pt, Anglais (États-Unis)

Mis en forme : Préformaté HTML, Gauche, Interligne : simple

Tableau mis en forme

Mis en forme : Police : +Corps (Calibri), 11 pt, Couleur de police : Texte 1

Mis en forme : Police : +Corps (Calibri), 11 pt, Couleur de police : Texte 1, Anglais (États-Unis)

Mis en forme : Police : +Corps (Calibri), 11 pt, Couleur de police : Texte 1, Anglais (États-Unis)

Mis en forme : Police : +Corps (Calibri), 11 pt, Couleur de police : Texte 1, Anglais (États-Unis)

23-December-2019	371	-31.7	-212
EPB24-December-2019	-6.24 ‰ ₃₆₇	-8.27 ‰ _{31.9}	-10.78 ‰ ₂₁₁
25-December-2019	378	-31.7	-211
26-December-2019	370	-31.7	-209
27-December-2019	386	-32.3	-208
NEEM28-December-2019	-33.5 ‰ ₃₇₀	-34.48 ‰ _{31.5}	-36.99 ‰ ₂₁₁
FP529-December-2019	-48.33 ‰ ₃₆₄	-49.02 ‰ _{31.5}	-51.53 ‰ ₂₀₉
30-December-2019	380	-31.7	-211
31-December-2019	372	-31.8	-211
1-January-2020	379	-31.8	-212
2-January-2020	371	-31.7	-211
3-January-2020	381	-31.6	-210
4-January-2020	378	-31.6	-210
5-January-2020	371	-31.6	-208

Table 3: Comparison of measured vs VSMOW calibrated $\delta^{18}\text{O}$ values for 3 standards measured with a Picarro analyzer after generation of water vapor humidity (1 σ over 10 minutes = 9 ppmv), $\delta^{18}\text{O}$ (1 σ over 10 minutes = 1.4 ‰), and δD (1 σ over 10 minutes = 4.5 ‰) of a laboratory standard (NEEM) using the LHLG.

We used the measured and true values of EPB and FP5 to estimate the $\delta^{18}\text{O}$ value of the NEEM standard from its measured value (Table 3). Using the linear relationship obtained from VSMOW calibrated EPB and FP5 $\delta^{18}\text{O}$ vs measured EPB and FP5 $\delta^{18}\text{O}$ values following the recommendations of the National Institute of Standards and Technology (NIST, reference material 8535a) leads to an estimated NEEM $\delta^{18}\text{O}$ of -33.31 ‰ to be compared to the independently VSMOW calibrated value of -33.5 ‰. Given the uncertainty of about 0.8-1 ‰ when measuring $\delta^{18}\text{O}$ around 800 ppmv, we can conclude that the system is accurate.

4- Application

The main application of this device is the interpretation of water isotopic profiles at dry sites, in particular in polar regions. As shown in Figure 5, the influence of humidity on the measurement of the water vapor isotopic composition with the L2130-i analyzer is large when humidity is below 12,000 ppm and increases when humidity decreases. Even though the precise isotope ratio-humidity calibration curve is likely to be

Mis en forme : Préformaté HTML, Gauche, Interligne : simple

Mis en forme : Police : +Corps (Calibri), 11 pt, Couleur de police : Texte 1

Tableau mis en forme

Mis en forme : Police : +Corps (Calibri), 11 pt, Couleur de police : Texte 1

Mis en forme : Police : +Corps (Calibri), 11 pt, Couleur de police : Texte 1

Mis en forme : Police : +Corps (Calibri), 11 pt, Couleur de police : Texte 1

Tableau mis en forme

Mis en forme : Police : +Corps (Calibri), 11 pt, Couleur de police : Texte 1

Mis en forme : Police : +Corps (Calibri), 11 pt, Couleur de police : Texte 1

Mis en forme : Police : +Corps (Calibri), 11 pt, Couleur de police : Texte 1

Mis en forme : Préformaté HTML, Gauche, Interligne : simple

Mis en forme : Police : +Corps (Calibri), 11 pt, Couleur de police : Texte 1

Mis en forme : Préformaté HTML, Gauche, Interligne : simple

Mis en forme : Police : +Corps (Calibri), 11 pt, Couleur de police : Texte 1

Mis en forme : Police : +Corps (Calibri), 11 pt, Couleur de police : Texte 1

Mis en forme : Police : +Corps (Calibri), 11 pt, Couleur de police : Texte 1

Mis en forme : Police : +Corps (Calibri), 11 pt, Couleur de police : Texte 1

Mis en forme : Police : +Corps (Calibri), 11 pt, Couleur de police : Texte 1

Mis en forme : Préformaté HTML, Gauche

Mis en forme : Police : +Corps (Calibri), 11 pt, Couleur de police : Texte 1, Anglais (États-Unis)

Mis en forme : Police : +Corps (Calibri), 11 pt, Couleur de police : Texte 1, Anglais (États-Unis)

Mis en forme : Police : +Corps (Calibri), 11 pt, Couleur de police : Texte 1, Anglais (États-Unis)

Mis en forme

Mis en forme : Préformaté HTML, Gauche

Mis en forme

Mis en forme

Mis en forme

different from one analyzer to another, all laser-based water isotope analyzers investigated to date have shown a strongly non-linear response at low-humidity levels (Guilpart et al., 2017; Leroy Dos-Santos, 2020; Weng et al., 2020). At the Concordia station, even in summer, humidity is generally below 1,000 ppmv (Figure 6) so that the interpretation of the diurnal variability of the water vapor isotopic composition is strongly affected by the dependency of the measured $\delta^{18}\text{O}$ and δD signals on humidity. Figure 6 displays such diurnal variabilities during austral summer 2018-2019 at Concordia and the consequently large correction of the isotopic records (uncorrected in grey and corrected in black).

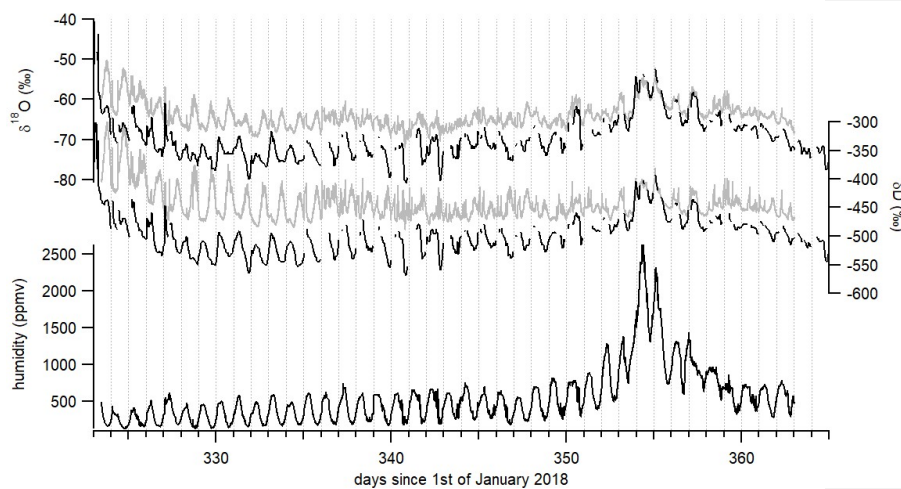


Figure 6: $\delta^{18}\text{O}$, δD and humidity records over December 2018 and beginning of January 2019. Raw isotopic values are in grey. Corrected isotopic values at hourly resolution are in black after correction of the influence of humidity on the water isotopic ratios and adjustment of $\delta^{18}\text{O}$ and δD values on the VSMOW-VSLAP scale using relationships between measured lab-standard values and known VSMOW calibrated lab-standard values. Removal of measurements performed during calibration or other maintenance operations.

The data clearly demonstrate the importance of the humidity correction which shifts the curves generally to lower isotopic ratio values. However, the difference between uncorrected and corrected data is particularly important in the observation of the diurnal variability, illustrated even better when zooming in on a section of the data, as in Figure 7. When looking in detail at the diurnal variability in the raw $\delta^{18}\text{O}$ and δD isotope data, some periods stand out with two identified daily peaks, one in phase with the humidity peak (marked in red in Figure 7) and one occurring during the period of minimum humidity (marked in blue in Figure 7). The strong non-linearity of the calibration curve of Figure 5 suggests that artificial peaks in $\delta^{18}\text{O}$ and δD could be due to changing humidity levels. Indeed, after correcting the data for the humidity dependence of the analyzer (black curve in Figure 7), the isotopic peaks occurring during

humidity minima are diminished or disappear altogether, while the peaks occurring during humidity maxima are amplified. More strikingly, the phase of the signal changes by practically 180° over some periods. Whereas the raw isotope signal peaks during the night, the corrected record shows higher isotope ratios during daytime. The diurnal variability recorded on both raw and corrected isotopic values during a period with higher humidity level, hence when the isotope ratio-humidity correction is smaller (around day 355 in figure 6), also shows that the $\delta^{18}\text{O}$ (δD) diurnal cycles are indeed in-phase with the humidity cycle. This result confirms the correlation between humidity cycles and $\delta^{18}\text{O}$ and δD of the water vapor at the daily scale at Concordia as reported by Casado et al. (2016). We thus conclude that the anticorrelation observed between $\delta^{18}\text{O}$ (δD) and humidity in the raw data (highlighted in blue in Figure 7) during periods of low-humidity is an artefact due to the influence of the humidity level on the vapor isotopic measurements by the L2130-i analyzer.

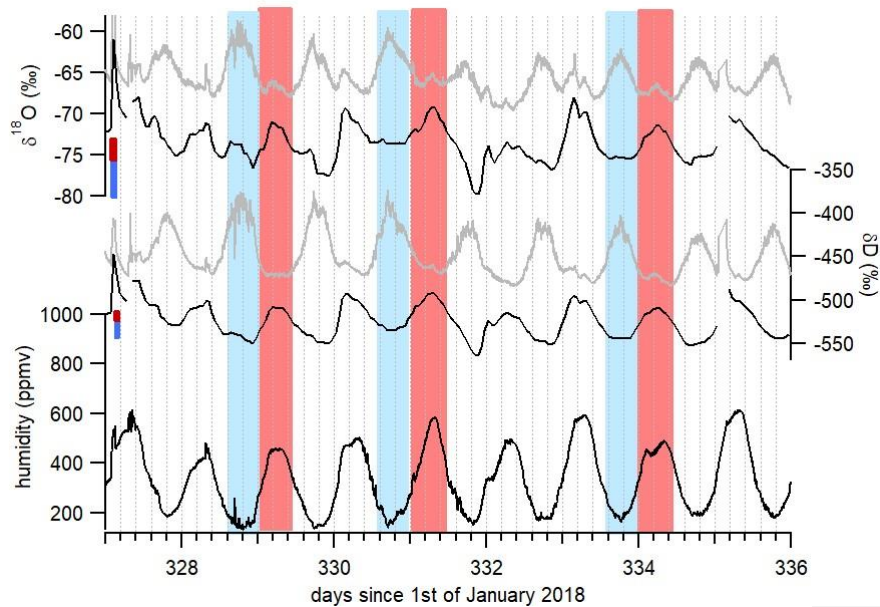


Figure 7: Focus on diurnal variability of $\delta^{18}\text{O}$, δD and humidity recorded at Concordia. Grey curves show the raw measurements and black curves the corrected records. The red (blue) bars indicate the calculated uncertainty due to the isotopic ratio vs humidity dependence (Figure 5) on the corrected $\delta^{18}\text{O}$ and δD values during periods with maximum (minimum) humidity. The red (blue) rectangles indicate half day with maximum (minimum) humidity.

5- Conclusion

We have developed an autonomous instrument for low-humidity generation (70 to 2,400 ppmv) with controlled water vapor isotopic composition specifically aimed at carrying out continuous measurements of the water vapor isotopic composition using a laser-based spectrometer in regions characterized by very low-humidity, such as polar regions. If needed, an interface permits to conveniently connect the new LHLG to the valve sequencer port of commercial Picarro instruments. After more than one year of routine operation on two Antarctic sites (Dumont d'Urville and Concordia), this instrument has proven to be very reliable and robust. It consistently generates stable humidity levels with a 1σ variability lower than 10 ppmv over more than 10 minutes. Besides, its performance is significantly better than that of the Picarro SDM at low humidity.

We used this instrument for the calibration of our water isotopic data with a special focus on accurately quantifying the influence of humidity on the measured isotopic composition of the water vapor. This effect is huge at low-humidity. We showed that this has an important impact on the interpretation of the diurnal cycles of $\delta^{18}\text{O}$ and δD in the water vapor at the Concordia station at humidity below 1,500 ppmv. We were able to confirm that, at this site, the diurnal $\delta^{18}\text{O}$ and δD variability is actually correlated with humidity variability, which would not have been possible without the new LHLG instrument.

Finally, the development of such an instrument is an important step forward to a better understanding of the transfer function between climate parameters and the isotopic composition of deep ice cores from the remote East Antarctic plateau, especially in the context of the new program "Beyond EPICA". It should be completed by ongoing development of laser spectrometers better adapted to low-humidity levels, such as those based on the technique of Optical Feedback Cavity Enhanced Absorption Spectroscopy (OFCEAS) (Casado et al., 2016; Landsberg, 2014; Landsberg et al., 2014).

Author contributions

CLDS, MC, FP and EK designed and built the instrument. OJ realized the software interface development. CLDS, MC and AL installed the instrument in Antarctica and tested it extensively. EK, SK, MF, AL and EF tested the instrument in the laboratory. AL wrote the manuscript with the help of all co-authors.

Acknowledgments

The development presented in this manuscript is largely inspired from the initial PhD work of Janek Landsberg which we gratefully acknowledge here. The research leading to these results has received funding from the Antarctic Snow program of the Fondation Prince Albert II de Monaco, the ANR EAIIST and CNRS-LEFE program ADELISE. The deployment of this instrument in the field was made possible through the logistic support of the NIVO2 & ADELISE IPEV programs. We thank the two reviewers for their useful comments which greatly improved the manuscript.

References

- Aemisegger, F., Sturm, P., Graf, P., Sodemann, H., Pfahl, S., Knohl, A. and Wernli, H.: Measuring variations $\delta^{18}\text{O}$ and $\delta^2\text{H}$ in atmospheric water vapour using two commercial laser-based spectrometers: an instrument characterisation study, *Atmos. Meas. Tech.*, 5(7), 1491–1511, doi:10.5194/amt-5-1491-2012, 2012.
- Bailey, H. L., Kaufman, D. S., Henderson, A. C. G. and Leng, M. J.: Synoptic scale controls on the $\delta^{18}\text{O}$ in precipitation across Beringia, *Geophys. Res. Lett.*, 42(11), 4608–4616, doi:10.1002/2015GL063983, Received, 2015.
- Bastrikov, V., Steen-Larsen, H. C., Masson-Delmotte, V., Gribanov, K., Cattani, O., Jouzel, J. and Zakharov, V.: Continuous measurements of atmospheric water vapour isotopes in western Siberia (Kourovka), *Atmos. Meas. Tech.*, 7(6), 1763–1776, doi:10.5194/amt-7-1763-2014, 2014.
- Bonne, J.-L., Masson-Delmotte, V., Cattani, O., Delmotte, M., Risi, C., Sodemann, H. and Steen-Larsen, H. C.: The isotopic composition of water vapour and precipitation in Ivittuut, southern Greenland, *Atmos. Chem. Phys.*, 14(9), 4419–4439, doi:10.5194/acp-14-4419-2014, 2014.
- Bréant, C., Leroy Dos Santos, C., Agosta, C., Casado, M., Fourré, E., Goursaud, S., Masson-Delmotte, V., Favier, V., Cattani, O., Prié, F., Golly, B., Orsi, A., Martinerie, P. and Landais, A.: Coastal water vapor isotopic composition driven by katabatic wind variability in summer at Dumont d’Urville, coastal East Antarctica, *Earth Planet. Sci. Lett.*, 514, 37–47, doi:10.1016/j.epsl.2019.03.004, 2019.
- ~~Cappa, C. D., Hendricks, M. B., DePaolo, D. J. and Cohen, R. C.: Isotopic fractionation of water during evaporation, *J. Geophys. Res.*, 108(D16), 4525, doi:10.1029/2003JD003597, 2003.~~
- Casado, M., Landais, A., Masson-Delmotte, V., Genthon, C., Kerstel, E., Kassi, S., Arnaud, L., Picard, G., Prié, F., Cattani, O., Steen-Larsen, H.-C., Vignon, E. and Cermak, P.: Continuous measurements of isotopic composition of water vapour on the East Antarctic Plateau, *Atmos. Chem. Phys. Discuss.*, 1–26, doi:10.5194/acp-2016-8, 2016.
- Casado, M., Landais, A., Picard, G., Münch, T., Laepple, T., Stenni, B., Dreossi, G., Ekaykin, A., Arnaud, L., Genthon, C., Touzeau, A., Masson-Delmotte, V. and Jouzel, J.: Archival processes of the water stable isotope signal in East Antarctic ice cores, *Cryosphere*, 12(5), doi:10.5194/tc-12-1745-2018, 2018.
- ~~Dong, F. Feng, and Douglas-Baer, D., 2010. “Development and Deployment of a Portable Water Isotope Analyzer for Accurate, Continuous and High-Frequency Oxygen and Hydrogen Isotope Measurements in Water Vapor and Liquid Water, in:” In Geophysical Research Abstracts, 12:EGU2010-5571, 2010.~~
- Ellehoj, M. D., Steen-Larsen, H. C., Johnsen, S. J. and Madsen, M. B.: Ice-vapor equilibrium fractionation factor of hydrogen and oxygen isotopes: Experimental investigations and implications for stable water isotope studies, *Rapid Commun. Mass Spectrom.*, 27(19), 2149–2158, doi:10.1002/rcm.6668, 2013.
- Genthon, C., Piard, L., Vignon, E., Madeleine, J.-B., Casado, M. and Gallée, H.: Atmospheric moisture supersaturation in the near-surface atmosphere at Dome C, Antarctic Plateau, *Atmos. Chem. Phys.*, 17(1), 691–704, doi:10.5194/acp-17-691-2017, 2017.
- Gkinis, V., Popp, T. J., Johnsen, S. J. and Blunier, T.: A continuous stream flash evaporator for the calibration of an IR cavity ring-down spectrometer for the isotopic analysis of water, *Isotopes Environ. Health Stud.*, 46(4), 463–475, doi:10.1080/10256016.2010.538052, 2010.
- Guilpart, E., Vimeux, F., Evan, S., Brioude, J., Metzger, J., Barthe, C., Risi, C. and Cattani, O.: The isotopic

composition of near-surface water vapor at the Maïdo observatory (Reunion Island, southwestern Indian Ocean) documents the controls of the humidity of the subtropical troposphere, *J. Geophys. Res. Atmos.*, 122(18), 9628–9650, doi:10.1002/2017JD026791, 2017.

Iannone, R., Romanini, D., Kass, S., Meijer, H. A. J. and Kerstel, E.: A Microdrop Generator for the Calibration of a Water Vapor Isotope Ratio Spectrometer, *J. Atmos. Ocean. Technol.*, 26, doi:10.1175/2008JTECHA1218.1, 2009.

Jouzel, J., Masson-Delmotte, V., Cattani, O., Dreyfus, G., Falourd, S., Hoffmann, G., Minster, B., Nouet, J., Barnola, J. M., Chappellaz, J., Fischer, H., Gallet, J. C., Johnsen, S., Leuenberger, M., Loulergue, L., Luthi, D., Oerter, H., Parrenin, F., Raisbeck, G., Raynaud, D., Schilt, a, Schwander, J., Selmo, E., Souchez, R., Spahni, R., Stauffer, B., Steffensen, J. P., Stenni, B., Stocker, T. F., Tison, J. L., Werner, M. and Wolff, E. W.: Orbital and millennial Antarctic climate variability over the past 800,000 years., *Science*, 317(5839), 793–796, doi:10.1126/science.1141038, 2007.

Kerstel, E. Modeling the Dynamic Behavior of a Droplet Evaporation Device for the Delivery of Isotopically Calibrated Low-Humidity Water Vapor, Atmospheric Measurement Techniques Discussions, 1–19.
<https://doi.org/10.5194/amt-2020-428>, 2020.

Kopeck, B., Lauder, A., Posmentier, E. and Feng, X.: The diel cycle of water vapor in west Greenland, *J. Geophys. Res. Atmos.*, 119(15), 9386–9399, 2014.

Landsberg, J.: Développement d'un spectromètre laser OF-CEAS pour les mesures des isotopes de la vapeur d'eau aux concentrations de l'eau basses. [online] Available from: <http://www.theses.fr/2014GRENOY052/document>, 2014.

Landsberg, J., Romanini, D. and Kerstel, E.: Very high finesse optical-feedback cavity-enhanced absorption spectrometer for low concentration water vapor isotope analyses., *Opt. Lett.*, 39(7), 1795–1798, doi:10.1364/OL.39.001795, 2014.

Lee, X., Sargent, S., Smith, R. and Tanner, B.: In Situ Measurement of the Water Vapor $^{18}\text{O}/^{16}\text{O}$ Isotope Ratio for Atmospheric and Ecological Applications, *J. Atmos. Ocean. Technol.*, 22(5), 555–565, doi:10.1175/JTECH1719.1, 2005.

Leroy Dos Santos, C., Masson-Delmotte, V., Casado, M., Fourré, E., Steen-Larsen, H-C, Maturilli, M., Orsi, A., Berchet, A., Cattani, O., Minster, B., Gherardi, J. and Landais, A., A 4.5 year-long record of Svalbard water vapor isotopic composition documents winter air mass origin, *J. Geophys. Research*, 125 (23),
(10.1029/2020JD032681), 2020.in-revision

Ritter, F., Steen-larsen, H. C., Werner, M., Masson-Delmotte, V., Orsi, A., Behrens, M., Birnbaum, G., Freitag, J., Risi, C. and Kipfstuhl, S.: Isotopic exchange on the diurnal scale between near-surface snow and lower atmospheric water vapor at Kohnen station , East Antarctica, *J. Geophys. Research* (February), 1–35, doi:10.5194/tc-2016-4, 2016.

Sayres, David S, E J Moyer, T F Hanisco, J M St Clair, F N Keutsch, A O'Brien, N T Allen, et al., A New Cavity Based Absorption Instrument for Detection of Water Isotopologues in the Upper Troposphere and Lower Stratosphere. Review of Scientific Instruments 80 (4): 44102–14.
<http://link.aip.org/link/?RSI/80/044102/1>, 2009.

Schmidt, M., Maseyk, K., Lett, C., Biron, P., Richard, P., Bariac, T. and Seibt, U.: Concentration effects on laser-based $\delta^{18}\text{O}$ and $\delta^2\text{H}$ measurements and implications for the calibration of vapour measurements with liquid standards, *Rapid Commun. Mass Spectrom.*, 24(24), 3553–3561, doi:10.1002/rcm.4813, 2010.

562 Sodemann, H., Aemisegger, F., Pfahl, S., Bitter, M., Corsmeier, U., Feuerle, T., Graf, P., Hankers, R., Hsiao,
 563 G., Schulz, H., Wieser, A. and Wernli, H.: The stable isotopic composition of water vapour above Corsica
 564 during the HyMeX SOP1 campaign: Insight into vertical mixing processes from lower-tropospheric survey
 565 flights, *Atmos. Chem. Phys.*, 17(9), 6125–6151, doi:10.5194/acp-17-6125-2017, 2017.

566 Steen-Larsen, H. C., Masson-Delmotte, V., Hirabayashi, M., Winkler, R., Satow, K., Prié, F., Bayou, N., Brun,
 567 E., Cuffey, K. M., Dahl-Jensen, D., Dumont, M., Guillevic, M., Kipfstuhl, S., Landais, A., Popp, T., Risi, C.,
 568 Steffen, K., Stenni, B. and Sveinbjörnsdóttir, A. E.: What controls the isotopic composition of Greenland
 569 surface snow?, *Clim. Past*, 10(1), 377–392, doi:10.5194/cp-10-377-2014, 2014.

570 Sturm, P. and Knohl, A.: Water vapor $\delta^2\text{H}$ and $\delta^{18}\text{O}$ measurements using off-axis integrated cavity output
 571 spectroscopy, *Atmos. Meas. Tech. Discuss.*, 2(4), 2055–2085, doi:10.5194/amtd-2-2055-2009, 2009.

572 Tremoy, G., Vimeux, F., Cattani, O., Mayaki, S., Souley, I. and Favreau, G.: Measurements of water vapor
 573 isotope ratios with wavelength-scanned cavity ring-down spectroscopy technology: new insights and
 574 important caveats for deuterium excess measurements in tropical areas in comparison with isotope-ratio
 575 mass spectrometry, *Rapid Commun. Mass Spectrom.*, 25(23), 3469–3480, doi:10.1002/rcm.5252, 2011.

576 Wang, L., Caylor, K. and Dragoni, D.: On the calibration of continuous, high-precision $\delta^{18}\text{O}$ and $\delta^2\text{H}$
 577 measurements using an off-axis integrated cavity output spectrometer, *Rapid Commun. Mass Spectrom.*,
 578 23, 530–536, doi:10.1002/rcm.3905, 2009.

579 Weng, Y., Touzeau, A. and Sodemann, H.: Impact of isotope composition on the humidity dependency
 580 correction of water vapour isotope measurements with infra-red cavity ring-down spectrometers, *Atmos.*
 581 *Meas. Tech.*, 13, 3167–3190, <https://doi.org/10.5194/amt-13-3167-2020>, 2020.

582
 583
 584
 585